Published in final edited form as:
J Vet Cardiol. 2011 June ; 13(2): 101–113. doi:10.1016/j.jvc.2011.03.002.

Ultrastructural changes in cardiac myocytes from Boxer dogs with arrhythmogenic right ventricular cardiomyopathy

Eva M. Oxford, PhD[a], **Charles G. Danko, PhD**[b], **Bruce G. Kornreich, DVM, PhD**[a], **Karen Maass, PhD**[c], **Shari A. Hemsley, BS**[a], **Dima Raskolnikov, BS**[a], **Philip R. Fox, DVM, MS**[d], **Mario Delmar, MD, PhD**[e], and **N. Sydney Moïse, DVM, MS**[a,*]

[a]College of Veterinary Medicine, Cornell University, Department of Clinical Sciences, Section of Cardiology, Ithaca, NY 14853, USA

[b]Cornell University, Department of Biological Statistics and Computational Biology, Ithaca, NY 14853, USA

[c]Leon H. Charney Division of Cardiology, New York University School of Medicine, New York, NY 10016, USA

[d]Caspary Institute, The Animal Medical Center, New York, NY 10065, USA

[e]Center for Arrhythmia Research, University of Michigan, Ann Arbor, MI 48109, USA

Abstract

Objectives—We sought to quantify the number and length of desmosomes, gap junctions, and adherens junctions in arrhythmogenic right ventricular cardiomyopathy (ARVC) and non-ARVC dogs, and to determine if ultrastructural changes existed.

Animals—Hearts from 8 boxer dogs afflicted with histopathologically confirmed ARVC and 6 dogs without ARVC were studied.

Methods—Quantitative transmission electron microscopy (TEM) and Western blot semi-quantification of α-actinin were used to study the intercalated disc and sarcomere of the right and left ventricles.

Results—When ARVC dogs were compared to non-ARVC dogs reductions in the number of desmosomes ($P = 0.04$), adherens junctions ($P = 0.04$) and gap junctions ($P = 0.02$) were found. The number of gap junctions ($P = 0.04$) and adherens junctions ($P = 0.04$) also were reduced in the left ventricle, while the number of desmosomes was not ($P = 0.88$). A decrease in the length of desmosomal complexes within LV samples ($P=0.04$) was found. These findings suggested disruption of proteins providing attachment of the cytoskeleton to the intercalated disc. Immunoblotting did not demonstrate a quantitative reduction in the amount of α-actinin in ARVC afflicted samples. All boxers with ARVC demonstrated the presence of electron dense material originating from the Z band and extending into the sarcomere, apparently at the expense of the cytoskeletal structure.

[*]**Corresponding author** nsm2@cornell.edu (N.S. Moise).

Conflict of interest
No conflict of interests for any of the authors.

Conclusions—These results emphasize the importance of structural integrity of the intercalated disc in the pathogenesis of ARVC. In addition, observed abnormalities in sarcomeric structure suggest a novel link between ARVC and the actin-myosin contractile apparatus.

Keywords

Canine; ARVC; Boxer; electron microscopy; desmosome; intercalated disc; cardiac ultrastructure

Introduction

Arrhythmogenic right ventricular cardiomyopathy (ARVC) is an inherited disease occurring in both humans and in the boxer dog.[1,2] In both, the mode of inheritance is considered to be autosomal dominant.[2,3] Clinical characteristics of ARVC are nearly identical in both human and boxer, including monomorphic left bundle branch block ventricular arrhythmias, heart failure, and sudden cardiac death.[1,4] Histopathologic features of ARVC include fatty or fibro-fatty replacement of myocardium beginning, and most severe, in the region of the right ventricle (RV) known as the triangle of dysplasia;[5] often progressing from epicardium toward the endocardial layer. In its natural course, histopathological manifestations encompass the entire right ventricular mass, and may also encroach into the left ventricle.[5] Of the few models of ARVC available, the boxer is the most comparable in its disease manifestations to human ARVC; as current mouse models do not incorporate mutations found within the human population, nor do they display as similar a clinical phenotype.

In humans, ARVC is considered to be a disease of the desmosome, a mechanical junction within the intercalated disc anchoring to the intermediate filaments.[2] The intercalated disc is comprised of 2 additional macromolecular components resolvable by electron microscopy: gap junctions provide a pathway for electrical and metabolic signaling between cells, and adherens junctions provide mechanical anchoring of actin filaments via cadherin molecules.[6] Immunofluorescence analysis of human ARVC-afflicted tissue reveals a characteristic histopathological profile that includes loss of immunoreactive plakoglobin (a desmosomal and adherens junction molecule) and connexin 43 (the cardiac gap junction protein of adult ventricle) at the site of the intercalated disc.[7] Similar findings have been reported in the ARVC afflicted boxer,[8] although no mutation was detected in the desmosomal genes that have been linked to human ARVC.[8] Recently an 8-bp deletion in the 3’ untranslated region of the striatin gene on chromosome 17 has been associated with ARVC in the boxer dog.[9] Further research is necessary to determine the mechanism by which this mutation is linked to ARVC. Though some ultrastructural information exists describing the intercalated disc of ARVC-afflicted human hearts,[10] extensive ultrastructural analysis of multiple, properly preserved samples is limited by the constraints intrinsic to human studies. Here, we hypothesize that the mislocalization of junctional proteins, seen through immunofluorescence in our previous study,[8] is an indication of the disorganization of gap junctions, desmosomes, and adherens junctions within the intercalated disc.

Animal, materials and methods

Animals

The investigation conformed to the *Guide for the Care and Use of Laboratory Animals* published by the US National Institutes of Health (NIH Publication No. 85–23, revised 1996), and was approved by Institutional Animal Care and Use Committee at Cornell University. Informed consent was obtained from the owners of client owned dogs prior to inclusion in the study. Animals were assigned arbitrary numbers in order to maintain confidentiality. Eight ARVC afflicted boxers were included in our study (2 females, 6 males). Due to the difficulty in finding non-ARVC boxers to study, six non-ARVC dogs of

other breeds were used as controls. The one beagle, and one German shepherd (Non-ARVC #5, see Table 1) of the non-ARVC group had no history of heart disease. The remaining German shepherds belonged to a colony previously identified as susceptible to inherited ventricular arrhythmias in animals less than 2 years of age.[11] These animals were used because they were age matched, and tissue was easily obtained immediately at death.

In humans, a diagnosis of ARVC is based on a set of major and minor criteria encompassing structural, electrocardiographic, and histological criteria that were most recently determined through the North American Multidisciplinary Study in 2009.[12] Such a diagnostic strategy has not as yet been defined in dogs. Therefore, we used a combination of electrocardiographic and histopathologic characteristics to confirm a phenotypic diagnosis of ARVC in the dogs studied.

Determination of phenotype

Antemortem evaluation consisted of 24-hour ambulatory electrocardiographic (Holter) monitoring and echocardiography. Ambulatory electrocardiography and analysis was performed using Trillium 5000 recorders and analysis package.f A three-lead orthogonal electrocardiographic configuration was used to produce a modified X, Y, and Z lead configuration as previously described.[13] Analysis of the Holter recordings was made by a veterinary cardiology technician highly trained to identify and quantify the number of arrhythmias. Most dogs had repeated 24-hour Holter monitoring; however, the data presented here is from a single recording. For the ARVC dogs, results are those from the recordings before treatment for arrhythmias and for the non-ARVC dogs results are those from the final recording made in the week prior to euthanasia. Two-dimensional and derived M mode echocardiography, color flow Doppler, and continuous wave spectral Doppler evaluations were performed with the dogs in lateral recumbency using a Vivid 7 Echocardiograph equipped with a 5S 2.2–5 MHz phased array sector probe.g Selected echocardiographic parameters that reflect myocardial size and function were reported. The LA/Ao ratio was determined from the 2-dimensional frame at the beginning of diastole as previously described.[14]

Tissue sample collection and histology

All boxers were client-owned animals and each was euthanized at the owners' request because of concurrent disease (n = 7) or heart disease (n = 1) for which the prognosis was poor. Following euthanasia with pentobarbital sodium (86 mg/kg IV),h hearts were collected via left thoracotomy from all dogs. Hearts were collected within one hour of death, and samples were fixed for both light and electron microscopy. First, full thickness RV and LV samples were fixed in 10% phosphate-buffered formalin for gross pathology, histopathology, and immunofluorescence. Second, full thickness RV and LV samples were removed using a 3 mm biopsy punch and fixed in Karnovsky's fixative (5% gluteraldehyde, 4% formaldehyde, in 0.08M sodium phosphate buffer)i for electron microscopy studies. Additional samples were collected using a 3 mm biopsy punch from the trapezius muscles of 2 non-ARVC dogs (Table 1, dogs 1 and 3), and from 3 ARVC dogs (Table 1, dogs 1, 5, 6), and fixed in Karnovsky's fixative. Table 2 summarizes the procedures for which each sample was used.

[f]Trillium 5000 recorder, Forest Medical, East Syracuse, NY
[g]Vivid 7 Echocardiograph, General Electric Medical Systems, Horten, Norway
[h]Fatal-Plus, Vortech Pharmaceutical
[i]Karnovsky's fixative, Electron Microscopy Sciences, Hatfield, PA

Pathology

All pathological methods are described in detail in our previous study,[8] and are discussed briefly below.

Gross Pathology—Hearts from 13 dogs (5 GS and 8 boxer dogs) were examined (PRF) without knowledge of antemortem diagnosis. All other studies described were performed before the gross and histopathological examinations were known. The beagle (non-ARVC dog 1) heart was used in alternate studies and was not available for routine pathological examination. Transverse, 5μm tissue sections were cut perpendicular to the longitudinal axis of the RV and LV chambers, one-third to two-thirds the distance distal from the atrioventricular valves toward the apex.

Histopathology—Full-thickness tissue blocks were removed from the anterior, lateral, and posterior RV; anterior, lateral and posterior LV; ventricular septum; and left and right atrial walls. Longitudinal samples were also taken at the RV outflow tract. Five μm thick sections of full-thickness, paraffin embedded tissue samples were cut and stained with hematoxylin and eosin and Masson trichrome stains.

Electron Microscopy

For this portion of the study, samples from all 8 ARVC dogs, and from non-ARVC dogs 1–6 were considered. All samples were fixed in Karnovsky's fixative at 4° C for a minimum of 48 hours to a maximum of 1 week. After fixation, samples were cut from midmyocardium, and processed as described previously.[15,16] Briefly, samples were washed in 0.1M sodium cacodylate buffer (pH 7.4), treated with osmium tetroxide, dehydrated, infiltrated using increasing concentrations of Araldite/Epon 812,[j] and embedded in Araldite/Epon 812. Tissue samples were sectioned to 75nm thickness and stained with uranyl acetate followed by Reynold's Lead Citrate, in an electron microscopy facility (Department of Pathology, SUNY Upstate Medical University). Images were taken using a Technai 12 Biotwin transmission electron microscope. All sections were scanned using various magnifications between 800X and 26000X. Special attention was given to the condition of the mitochondria, in order to control for artifacts that would result from sample degradation. Samples used in this study all had well preserved mitochondrial architecture. Analysis of intercalated disc structures followed a protocol similar to that of Hoyt et al.[15] In summary, for each section, overviews from 3–5 different fields were taken at 1900X. Fields were chosen based on quality of longitudinal sectioning, lack of adipocyte infiltration (in ARVC dogs), and high quantity of intercalated discs. From each dog, an average of 6 intercalated discs (each spanning between 100–900 μm) within the 3–5 fields were considered. Images obtained at 13000X magnification followed the course of the intercalated discs included within the overview image. Images were analyzed using Image J 1.38X softwarek by a technician blinded to the clinical diagnosis of the canines. For each 13000X field of view, the following parameters were measured: individual intercalated disc length, number and length of gap junctions, desmosomes, and adherens junctions. The number of junctions was further quantified per 10 microns of intercalated disc. Structures were measured by following the curvature of the intercalated disc. Desmosomes were identified as structures formed from two dark, well-defined, parallel plaques containing an intercellular gap of approximately 30 nm. Adherens junctions were identified as two thick plaques with less distinct edges, on either side of a 30 nm intercellular gap. Gap junctions were identified as thick, dark structures, often at the ends of the intercalated disc, containing no intercellular

[j]Araldite/Epon 812, Electron Microscopy Sciences, Hatfield, PA
[k]Image processing and Analysis in Java by NIH Image.

gap. Gaps between the intercalated disc and the actin filaments were measured at 5 different areas in each of 3 fields in the ARVC and non-ARVC dogs.

Western blot

Frozen RV tissue samples from three boxers (Table 1, dogs 4, 5, and 7) and 2 non-ARVC dogs (Table 1, dogs 1 and 5) were homogenized in Laemmli buffer, and whole protein amounts measured by a Lowry protein assay. Proteins were separated by SDS-PAGE using an 8–16% tris-glycine gradient gel,l transferred onto nitrocellulose, blocked for 1 hour at room temperature with 0.5% non-fat milk in phosphate buffered saline (PBS), with .5% Tween, and probed with a monoclonal mouse anti-α-actinin (Sigma).m To ensure equal loading, blots were stripped with Restore Western Blot Stripping Buffer,n and incubated with primary monoclonal antibody to α cardiac actin.o

Statistical Analysis

Through the use of Shapiro-Wilk tests and examination of histograms, it was evident that data from several parameters were not normally distributed. Therefore, a Mann-Whitney U test was used for all comparisons. As previous studies demonstrate that intercalated disc components are lost in ARVC afflicted boxers,[8] one-sided tests were used. All results were corrected for multiple hypotheses testing using the Benjamini Hochberg (BH) false discovery rate.[19] All comparisons with a BH corrected P-value <0.05 were considered significant. Box plots were created using the default graphical parameters in the R statistical package v.2.9.[20]. Boxes delineate the 25th and 75th percentile, and a bisecting line marks the median. Whiskers show the maximum points that lie within 1.5 times the interquartile range; all data outside of this range are shown as points. All points are shown on each plot. Additionally, two-sided Mann-Whitney U tests were used in the comparison of age and weight in the ARVC and non-ARVC dogs.

Results

Determination of phenotype

Clinical Determination—ARVC and non-ARVC dogs were not significantly different in age (P=0.22) or weight (P=0.07) (Table 1). Seven of 8 boxers with ARVC and 5 of 6 dogs without ARVC had complete evaluations by echocardiography and Holter monitoring (Table 1). Five of the seven ARVC dogs had severe ventricular arrhythmias that required antiarrhythmic treatment. The ventricular arrhythmias were composed of greater than 85% monomorphic ectopy with a left bundle branch pattern. This pattern is characteristic of boxer dogs afflicted with ARVC.[21] Each of the dogs being treated had syncopal episodes. One boxer (#6) had infrequent premature ventricular complexes without ventricular tachycardia, but was determined to be affected during the blinded histopathological examination (see below). The five German shepherd dogs had infrequent ventricular premature complexes. As is characteristic of the inherited arrhythmias in this breed, the number of arrhythmias is negligible after 2 years of age.[22] Each of these non-ARVC dogs, except for non-ARVC dog 5, had severe ventricular arrhythmias including ventricular tachycardia documented before the age of 1 year. Non-ARVC dog 5 was a normal German shepherd and not related to the other German shepherd dogs with inherited ventricular arrhythmias.

[l]8–16% tris-glycine gradient gel, Invitrogen, Carlsbad, CA
[m]Monoclonal α-actinin antibody, Sigma Aldrich, St. Louis, MO
[n]Restore Western Blot Stripping Buffer, Pierce, Thermo Fisher Scientific, Rockford, IL
[o]Monoclonal antibody to α cardiac actin, Fitzgerald Industries International, North Acton, MA

Only one dog (ARVC dog 5) required treatment (pimobendan) for impaired systolic function evidenced by a marked reduction in the fractional shortening (Table 1). The RV was not assessed for the presence of myocardial dysfunction. Two boxers had LV free wall hypertrophy associated with concomitant aortic valve stenosis as identified by echocardiography and Doppler measurements indicating elevated gradients across the valve [ARVC dogs 3 (90 mmHg) and 6 (50 mmHg)]. None of the German shepherds had evidence of congestive heart failure. The beagle had a normal cardiovascular physical examination.

Pathologic findings—Each of the eight boxer dogs displayed histopathologic lesions that were characteristic of ARVC, [1,8,23] and have been described in detail in our previous study.[8] The most distinguishing features included substantial replacement of RV cardiac myocytes by adipose or fibrous tissue, which occurred in two patterns. The fatty form was characterized by diffusely distributed, multi-focal regions of adipose cell replacement within the RV wall and trabeculae, extending from epicardium toward endocardium, often in association with mild interstitial fibrosis. The fibro-fatty form consisted of focal or diffuse regions of adipose cell replacement associated with areas of mild replacement fibrosis. Both the fatty and fibro-fatty forms were characterized by residual surviving myocytes embedded within regions of fat, and fatty and fibrous tissue, respectively. Myocarditis characterized by focal or multifocal lymphocytic infiltrates and associated with myocyte death, was identified in the RV of three boxer dogs and one control dog. Coexisting aortic stenosis (ARVC dogs 3 and 6) diagnosed by echocardiography was confirmed by postmortem examination.

Ultrastructural Findings

Myocardium—Electron microscopic images revealed adipocytes interposed between myoctyes in all ventricular samples from ARVC-afflicted boxers, but not in the samples from the control group (Fig. 1; panel A obtained from control; panels B and C, from ARVC-afflicted hearts). These cells were found even in regions that did not appear to have fibrofatty infiltration per gross examination of the heart. No fibroblasts or other non-myocyte cell types were observed in the areas of adipocyte infiltrations. Higher magnification of the area of contact between myocytes and adipocytes did not reveal junctional structures between the two cell types, even in the region adjacent to the intercalated disc (Fig. 1, Panel C). In addition, no obvious junctions were present between adjacent adipocytes.

Intercalated disc—Quantitative TEM was used to characterize intercellular junctions in tissue sections from ARVC and non-ARVC dogs. Figure 2 shows representative electron micrographs of the intercalated discs of non-ARVC and ARVC afflicted tissue. The three macromolecular complexes of the intercalated disc: gap junctions, desmosomes, and adherens junctions, were present in all samples. No significant differences were detected ($P > 0.05$ BH corrected Mann Whitney U test, see methods) in the length of desmosomes, gap junctions, or adherens junctions measured in RV samples from ARVC or non-ARVC dogs [desmosomes, $P=0.7$ (ARVC: Median, 0.18, Range, 0.10–0.23; Non-ARVC: Median, 0.17, Range, 0.12–0.22), adherens junctions, $P=0.83$ (ARVC: Median, 0.28, Range, 0.24–0.36; Non-ARVC: Median, 0.28, Range, 0.17–0.39), gap junctions, $P=0.09$ (ARVC: Median, 0.42, Range, 0.14–1.34; Non-ARVC: Median, 0.48, Range, 0.09–1.20)]. Furthermore, no significant differences were detected in the length of adherens junctions or gap junctions measured in LV samples (adherens junctions, $P=0.83$ (ARVC: Median, 0.27, Range, 0.17–0.52; Non-ARVC: Median, 0.28, Range, 0.17–0.63), gap junctions, $P=0.7$ (ARVC: Median, 0.43, Range, 0.10–1.25; Non-ARVC: Median, 0.45, Range, 0.13–1.40). Interestingly, as shown in figure 3, a significant decrease in the length of desmosomal complexes within LV samples from ARVC dogs was noted, compared to non-ARVC dogs ($P=0.04$).

While the size of the junctional structures in the right ventricle was not different in the affected hearts, the number of those complexes (per 10 μm of intercalated disc membrane) was significantly reduced. Figure 4 shows the results. Statistical analysis yielded *P* values of, respectively, 0.04, 0.04 and 0.02 for the reduction in the number of desmosomes, adherens junctions and gap junctions measured. The number of gap junctions and adherens junctions were also reduced in the left ventricle (*P*=0.04 in both cases), while the number of desmosomes was not significantly affected (*P* =0.88). Taken together, these results suggest that remodeling occurred within the intercalated disc in the myocardium of ARVC dogs.

Cytoskeletal-intercalated disc coupling—Adherens junctions couple to the cytoskeleton to create a mechanical continuum between cells. Thus, the changes observed in the abundance of adherens junctions led us to analyze the ultrastructural characteristics of the actin filaments at the sub-junctional space. Figure 2 depicts images of the area around the intercalated disc in one non-ARVC and three different ARVC dogs (dogs 3, 7, 8). In contrast to non-ARVC samples, myocytes from all ARVC-afflicted dogs showed a widening of the gap separating the end of well-defined actin filaments from the intercalated disc membrane (see, e.g., Figure 2, ARVC dogs 3 and 7); in these cases, the sub-sarcolemmal space was occupied by poorly organized, heterogeneous material, with actin filaments ending 0.25 to 1.5 microns away from the membrane of the cell. In some samples (Figure 2, ARVC dog 8), the intercalated disc appeared disorganized and folded upon itself, further suggesting a loss of the native structure. Sub-junctional annular structures were also observed (see white arrow in top right panel). These structures have been described before[24] and their abundance linked to junctional remodeling.[24] Overall, the data are indicative of a disruption in the interaction of the cytoskeletal structure with mechanical junctions at the intercalated disc.

Previous studies have shown that the coupling between adherens junctions and actin filaments is mediated, at least in part, by cytoskeletal adaptor proteins.[25] Among them, α-actinin has been previously shown to colocalize with adherens junctions proteins at the intercalated disc,[26] where it acts as the link between adherens junctions and the actin filament. A Western blot revealed no change in the total amount of α-actinin in tissue from 2 non-ARVC dogs compared to 3 ARVC afflicted boxers (Fig. 5).

Sarcomeric Ultrastructure—We next assessed the sarcomeric ultrastructure of ARVC dogs, compared to non-ARVC dogs. Figure 6 shows representative electron micrographs from the heart of a non-ARVC dog (dog 5), and three ARVC dogs (dogs 8, 2, 1). Proper alignment of sarcomeres, Z bands, and myofilaments was observed in all samples from non-ARVC dogs, including those that had a previous history of arrhythmias. Proper ultrastructural alignment was also observed in most areas of ARVC-afflicted tissue free of fatty or fibrofatty infiltration. However, in all cases of ARVC, sarcomeric alignment was interrupted by electron dense material originating at or around the Z band and displaying one or more of the following three patterns: 1) Electron dense material filling the entire area of alternating sarcomeres along a myofibril. 2) Electron dense material filling the entire area of every sarcomere in a multidirectional cluster. 3) Electron dense material appearing to originate at (or from) the Z bands and moving toward the center of the sarcomere, which did not appear to be affected. Similar electron dense material, coined “nemaline rods”, or “Z-band streaming”, is the hallmark of the human skeletal muscle disease, nemaline myopathy (for reviews see reference 27).[27] In these cases, it has been shown that an accumulation of α-actinin within the sarcomere is the main component of this electron dense material.[28] Due to the ultrastructural similarities between nemaline myopathy and our ARVC heart samples, we further explored the Z band streaming in samples from skeletal muscle.

Z bands were examined in the trapezius muscle of three ARVC dogs (dogs 1, 5, 6), and two non-ARVC dogs (dogs 1, 3) (data not shown). No electron dense rods, or other abnormalities, were detected in these skeletal muscle samples, thus suggesting that the sarcomeric anomaly observed in the boxer dogs was unique to the heart. The latter is consistent with the absence of skeletal muscle manifestations in the phenotype of these animals.

Discussion

Here, we report quantitative transmission electron microscopy (TEM) data demonstrating a decrease in the abundance of desmosomes, gap junctions, and adherens junctions in the left and right ventricles in boxers afflicted with ARVC. Moreover, we conducted an extensive analysis of the sarcomeric structure in ARVC samples and identified the presence of wide streaks of electron-dense material originating from and extending beyond the Z band structure. These modifications suggest a previously unidentified involvement of sarcomeric proteins in the pathology of (at least some cases of) ARVC. Overall, our data significantly expand current knowledge on the molecular substrate underlying this structural disease, and provide a foundation for future studies on the pathophysiological mechanisms leading to the clinical phenotype of ARVC.

This study reveals differences in the macromolecular composition of the intercalated disc in ARVC afflicted boxers. We observed a significant reduction in number, but not length, of gap junctions, desmosomes, and adherens junctions within the intercalated disc in RV samples from ARVC dogs compared to those from non-ARVC dogs. In the LV, a significant reduction in number, but not length, of both gap junctions and adherens junctions was observed in samples from ARVC dogs, compared to those from non-ARVC dogs. Interestingly, a significant decrease in length, but not number, of desmosomal plaques was detected in the LV samples from ARVC dogs, compared to samples from non-ARVC dogs.

It is worth mentioning that desmosomes and adherens junctions in the adult mammalian heart share molecular components and even structural characteristics, thus leading to their redefinition as a single “area composita”. [29] Yet, structures that displayed “classic” desmosomal morphology were identifiable in these adult canine hearts and were evaluated separately, given their importance in the context of ARVC.

Immunofluorescent microscopy studies previously documented reduced signals for desmosomal, adherens junctions, and gap junction proteins at the intercalated disc in both boxer dogs[8] and humans afflicted with ARVC.[17,18] Those studies used tissue from the LV, as it was less affected by fat and fibrous infiltrate. Our data are consistent with those previous findings, [4,17,18] as changes in either abundance or length of junctional plaques could translate in decreased signals detected by immunofluorescence. Furthermore, our EM studies make an interesting distinction: While adherens junctions and gap junctions decreased in abundance (numbers per 10 μm of ID), desmosomes decreased in length. This suggests that, though desmosomal proteins do not appear mutated in canine ARVC, the integrity of each desmosomal complex is, indeed, disrupted. At least one previous study suggests that increased clustering of desmosomes at the intercalated disc results in increased stability of the plaque.[30] Therefore, a decrease in the length of desmosomal plaques, as observed in the ARVC dogs, suggests a decrease in stability of the complexes. Changes in the numbers of gap and adherens junctions may be an indirect consequence of the loss of mechanical stability between cells, rather than on the ability of the relevant proteins to aggregate and stabilize each plaque.

We observed, through TEM, what appeared to be an increased separation of actin filaments from the intercalated disc in ARVC afflicted samples. Additionally, electron microscopy showed a loss of cytoskeletal organization in the subsarcolemmal space in ARVC-afflicted samples. These results suggest that both proteins of the intercalated disc, as well as those affiliated with the actin filament, are affected in cases of ARVC. Whether mislocalization of one group of proteins is consequent to the other, or the events occur independently, is to be determined in future studies.

Several abnormalities within the sarcomere were observed in ARVC afflicted tissue. Careful examination of high-resolution EM images revealed the accumulation of electron dense material appearing to originate at or around the Z bands; in both RV and LV samples from all ARVC dogs. These lesions were not observed in identically prepared control samples, and suggest that structural components of the cytoskeleton may be involved in the course of the disease. This electron dense material is not described in cases of human ARVC[10] and represents the first distinct phenotypic difference between human and boxer ARVC. Whether or not these lesions remain to be found in humans, or distinguish boxer ARVC as a separate and distinct disease is not yet understood.

The presence of similar electron dense material in skeletal muscle is the hallmark of the human disorder nemaline myopathy, a disease characterized by progressive skeletal muscle weakness and respiratory problems.[31] Nemaline myopathy results from genetic mutations in actin thin filament proteins.[31] Interestingly, cardiomyopathy has been reported in several cases of nemaline myopathy. [32–34] ARVC afflicted boxers have no known clinical, or histopathologic, history of skeletal muscle disease; however, actin filament proteins exist in different isoforms within heart and skeletal muscle. In cases of nemaline myopathy, immunogold electron microscopy studies revealed that aggregation of α-actinin within sarcomeres was the major contributor to the electron dense material.[28]

A Western blot revealed no quantifiable decrease in the total amount of α-actinin in ARVC affected samples. However, this does not rule out the possibility of a mislocalization of α-actinin within the cell, which may play a role in the loss of attachment of actin filaments at the intercalated disc.

An estimated 50% of cases of human ARVC have not yet been linked to a genetic mutation.[35] In addition; the fundamental mechanisms leading to ARVC remain unknown. Uncovering the molecular mechanisms leading to ARVC in boxer dogs may provide clues to both the pathophysiology of the disease, and the discovery of additional genes associated with ARVC. Our current data characterize components of the intercalated disc and of the sarcomeric unit in ARVC-afflicted hearts. We further identify a novel ultrastructural abnormality within the sarcomere not reported in the human population: a disruption of sarcomeric integrity associated with the clinical syndrome of ARVC in the afflicted boxer dog. Remodeling at both the intercalated disc and the sarcomere suggest that a fundamental pathway may exist between components of the intercalated disc and those of the cytoskeleton may exist.

The number of dogs available for study was limited, and, therefore, general conclusions about a disease process must be considered in this context. However, distinct and similar ultrastructural abnormalities were identified in all ARVC afflicted boxers, and in none of the dogs in our control group. In our ARVC population of boxers, 2 dogs had coexisting aortic stenosis; however, both of these dogs had ventricular arrhythmias with a left bundle branch block pattern suggesting origin from the right ventricle and confirmed histopathologic diagnoses of ARVC. Our control group consisted of five German shepherds and one beagle. Four of the German shepherds were afflicted with another inherited arrhythmic disorder,

however no comparable lesions were noted in the German shepherd EM samples when compared to those afflicted with ARVC. The need to obtain the hearts immediately after death limited the availability for a diverse group of dogs of many breeds. Therefore, it is possible that the reduction of macromolecular complexes of the intercalated disc, as well as the sarcomeric disturbances, could be specific abnormalities of the boxer breed. However, in humans, both abnormalities are apparent only in disease states. It therefore seems plausible to consider that these abnormalities are related to the presence of ARVC, rather than specific to the boxer breed.

Apparent losses of attachment were observed between the intercalated disc and the actin filaments in ARVC afflicted dogs. Due to the limited sample size, we were unable to quantify this finding. Although it is tempting to speculate that ARVC in the boxer dog is associated with a loss of attachment of the actin filaments to the intercalated disc, this may be an incidental finding.

An additional limitation to our study is the possibility of postmortem changes to the tissue. To minimize this possibility, each ARVC afflicted sample was treated from start to finish with a non-ARVC sample. In examining each sample, special care was given to the quality of the mitochondria, as swollen or damaged organelles is suggestive of postmortem damage or improper fixation. Additionally, each ARVC sample was closely compared to controls to eliminate the change of artifactual changes, which would have presumably affected non-ARVC as well as ARVC samples.

Finally, our data show the first distinct phenotypic difference between the human and boxer forms of ARVC. Our previous studies revealed that the genetic mutations commonly resulting in an ARVC phenotype in humans were not present in the boxer.[8] Further research in both human and boxer ARVC must be conducted in order to determine whether the boxer is an adequate model of human ARVC.

Limitations notwithstanding, we conclude that major abnormalities exist within both the intercalated disc and the sarcomere of ARVC afflicted dogs. These deficiencies may result in the loss of attachment of the cytoskeletal apparatus to points of cell-cell apposition and, accordingly, decreased electrical and mechanical communication between cardiac myocytes.

Acknowledgments

We wish to thank the clients who donated the hearts of their beloved pets to our study. We are grateful to our electron microscopy technician, Maureen Barcza for her sharing her expertise. Additionally, we thank Drs. Karen Vikstrom, Hollis Erb, and Fred Clubb for their thoughtful conversations.

Funding

This work was supported by grants from the Morris Animal Foundation [grant number D06CA-059] to [NSM]; the National Institutes of Health [grant number PO1-HL087226] to [MD]; and the Cornell Veterinary Investigator Program - Merck-Merial Program to [EMO].

Abbreviations

ARVC	Arrhythmogenic Right Ventricular Cardiomyopathy
BH	Benjamin Hochberg
EM	Electron Microscopy
ID	Intercalated Disc
LA/Ao	Left Atrium/Aorta

LV	Left Ventricle
PBS	Phosphate buffered saline
RV	Right Ventricle
TEM	Transmission Electron Microscopy

References

1. Basso C, Fox PR, Meurs KM, Towbin JA, Spier AW, Calabrese F, Maron BJ, Thiene G. Arrhythmogenic right ventricular cardiomyopathy causing sudden cardiac death in boxer dogs: a new animal model of human disease. Circulation. 2004; 109:1180–1185. [PubMed: 14993138]
2. Sen-Chowdhry S, Syrris P, McKenna WJ. Genetics of right ventricular cardiomyopathy. J Cardiovasc Electrophysiol. 2005; 16:927–935. [PubMed: 16101641]
3. Meurs KM. Boxer dog cardiomyopathy: an update. Vet Clin North Am Small Anim Pract. 2004; 34:1235–1244. viii. [PubMed: 15325480]
4. Sen-Chowdhry S, Morgan RD, Chambers JC, McKenna WJ. Arrhythmogenic cardiomyopathy: etiology, diagnosis, and treatment. Annu Rev Med. 2010; 61:233–253. [PubMed: 20059337]
5. Corrado D, Basso C, Thiene G, McKenna WJ, Davies MJ, Fontaliran F, Nava A, Silvestri F, Blomstrom-Lundqvist C, Wlodarska EK, Fontaine G, Camerini F. Spectrum of clinicopathologic manifestations of arrhythmogenic right ventricular cardiomyopathy/dysplasia: a multicenter study. J Am Coll Cardiol. 1997; 30:1512–1520. [PubMed: 9362410]
6. Volk T, Geiger B. A-CAM: a 135-kD receptor of intercellular adherens junctions. I. Immunoelectron microscopic localization and biochemical studies. J Cell Biol. 1986; 103:1441–1450. [PubMed: 3533954]
7. Asimaki A, Tandri H, Huang H, Halushka MK, Gautam S, Basso C, Thiene G, Tsatsopoulou A, Protonotarios N, McKenna WJ, Calkins H, Saffitz JE. A new diagnostic test for arrhythmogenic right ventricular cardiomyopathy. N Engl J Med. 2009; 360:1075–1084. [PubMed: 19279339]
8. Oxford EM, Everitt M, Coombs W, Fox PR, Kraus M, Gelzer AR, Saffitz J, Taffet SM, Moise NS, Delmar M. Molecular composition of the intercalated disc in a spontaneous canine animal model of arrhythmogenic right ventricular dysplasia/cardiomyopathy. Heart Rhythm. 2007; 4:1196–1205. [PubMed: 17765621]
9. Meurs KM, Mauceli E, Lahmers S, Acland GM, White SN, Lindblad-Toh K. Genome-wide association identifies a deletion in the 3' untranslated region of striatin in a canine model of arrhythmogenic right ventricular cardiomyopathy. Hum Genet. 2010; 128(3):315–324. [PubMed: 20596727]
10. Basso C, Czarnowska E, Della Barbera M, Bauce B, Beffagna G, Wlodarska EK, Pilichou K, Ramondo A, Lorenzon A, Wozniek O, Corrado D, Daliento L, Danieli GA, Valente M, Nava A, Thiene G, Rampazzo A. Ultrastructural evidence of intercalated disc remodelling in arrhythmogenic right ventricular cardiomyopathy: an electron microscopy investigation on endomyocardial biopsies. Eur Heart J. 2006; 27:1847–1854. [PubMed: 16774985]
11. Moise NS, Meyers-Wallen V, Flahive WJ, Valentine BA, Scarlett JM, Brown CA, Chavkin MJ, Dugger DA, Renaud-Farrell S, Kornreich B. Inherited ventricular arrhythmias and sudden death in German shepherd dogs. J Am Coll Cardiol. 1994; 24:233–243. [PubMed: 8006271]
12. Marcus FI, McKenna WJ, Sherrill D, Basso C, Bauce B, Bluemke DA, Calkins H, Corrado D, Cox MG, Daubert JP, Fontaine G, Gear K, Hauer R, Nava A, Picard MH, Protonotarios N, Saffitz JE, Sanborn DM, Steinberg JS, Tandri H, Thiene G, Towbin JA, Tsatsopoulou A, Wichter T, Zareba W. Diagnosis of arrhythmogenic right ventricular cardiomyopathy/dysplasia: proposed modification of the task force criteria. Circulation. 2010; 121:1533–1541. [PubMed: 20172911]
13. Moïse NS, Brittain DD, Flahive WJ Jr, Riccio ML, Ernst RS, Scarlett J, Mohammed HO, Morrison AR, Gilmour RF Jr. Relationship of ventricular tachycardia to sleep/wakefulness in a model of sudden cardiac death. Pediatr Res. 1996; 40:344–350. [PubMed: 8827788]
14. Rishniw M, Erb HN. Evaluation of Four 2-Dimensional Echocardiographic Methods of Assessing Left Atrial Size in Dogs. J Vet Intern Med. 2000; 14:429–435. [PubMed: 10935894]

15. Hoyt RH, Cohen ML, Saffitz JE. Distribution and three-dimensional structure of intercellular junctions in canine myocardium. Circ Res. 1989; 64:563–574. [PubMed: 2645060]
16. Hayat MA. Principles and techniques of electron microscopy: biological applications. 1989; 469
17. Kaplan SR, Gard JJ, Carvajal-Huerta L, Ruiz-Cabezas JC, Thiene G, Saffitz JE. Structural and molecular pathology of the heart in Carvajal syndrome. Cardiovasc Pathol. 2004; 13:26–32. [PubMed: 14761782]
18. Kaplan SR, Gard JJ, Protonotarios N, Tsatsopoulou A, Spiliopoulou C, Anastasakis A, Squarcioni CP, McKenna WJ, Thiene G, Basso C, Brousse N, Fontaine G, Saffitz JE. Remodeling of myocyte gap junctions in arrhythmogenic right ventricular cardiomyopathy due to a deletion in plakoglobin (Naxos disease). Heart Rhythm. 2004; 1:3–11. [PubMed: 15851108]
19. Benjamini Y, Hochberg Y. Controlling the false discovery rate: a practical and powerful approach to multiple testing. J R Statist Soc B. 1995; 1:289–300.
20. R Development Core Team. R: A Language and Environment for Statistical Computing. R Foundation For Statistical Computing. 2009 ISBN 3-900051-07-0; http://www.R-project.org.
21. Kraus MS, Moise NS, Rishniw M, Dykes N, Erb HN. Morphology of ventricular arrhythmias in the boxer as measured by 12-lead electrocardiography with pace-mapping comparison. J Vet Intern Med. 2002; 16:153–158. [PubMed: 11899030]
22. Moïse NS, Riccio ML, Kornreich B, Flahive WJ Jr, Gilmour RF Jr. Age dependence of the development of ventricular arrhythmias in a canine model of sudden cardiac death. Cardiovasc Res. 1997; 34:483–492. [PubMed: 9231031]
23. Fontaine G, Fontaliran F, Frank R. Arrhythmogenic right ventricular cardiomyopathies: clinical forms and main differential diagnoses. Circulation. 1998; 97:1532–1535. [PubMed: 9593556]
24. Hesketh GG, Shah MH, Halperin VL, Cooke CA, Akar FG, Yen TE, Kass DA, Machamer CE, Van Eyk JE, Tomaselli GF. Ultrastructure and regulation of lateralized connexin43 in the failing heart. Circ Res. 2010; 106:1153–1163. [PubMed: 20167932]
25. Niessen CM, Gottardi CJ. Molecular components of the adherens junction. Biochim Biophys Acta. 2008; 1778:562–571. [PubMed: 18206110]
26. Knudsen KA, Soler AP, Johnson KR, Wheelock MJ. Interaction of alpha-actinin with the cadherin/catenin cell-cell adhesion complex via alpha-catenin. J Cell Biol. 1995; 130:67–77. [PubMed: 7790378]
27. Sanoudou D, Beggs AH. Clinical and genetic heterogeneity in nemaline myopathy--a disease of skeletal muscle thin filaments. Trends Mol Med. 2001; 7:362–368. [PubMed: 11516997]
28. Jennekens FG, Roord JJ, Veldman H, Willemse J, Jockusch BM. Congenital nemaline myopathy. I. Defective organization of alpha-actinin is restricted to muscle. Muscle Nerve. 1983; 6:61–68. [PubMed: 6302502]
29. Franke WW, Borrmann CM, Grund C, Pieperhoff S. The area composita of adhering junctions connecting heart muscle cells of vertebrates. I. Molecular definition in intercalated disks of cardiomyocytes by immunoelectron microscopy of desmosomal proteins. Eur J Cell Biol. 2006; 85:69–82. [PubMed: 16406610]
30. Yap AS, Brieher WM, Pruschy M, Gumbiner BM. Lateral clustering of the adhesive ectodomain: a fundamental determinant of cadherin function. Curr Biol. 1997; 7:308–315. [PubMed: 9133345]
31. Clarkson E, Costa CF, Machesky LM. Congenital myopathies: diseases of the actin cytoskeleton. J Pathol. 2004; 204:407–417. [PubMed: 15495263]
32. Skyllouriotis ML, Marx M, Skyllouriotis P, Bittner R, Wimmer M. Nemaline myopathy and cardiomyopathy. Pediatr Neurol. 1999; 20:319–321. [PubMed: 10328285]
33. D'Amico A, Graziano C, Pacileo G, Petrini S, Nowak KJ, Boldrini R, Jacques A, Feng JJ, Porfirio B, Sewry CA, Santorelli FM, Limongelli G, Bertini E, Laing N, Marston SB. Fatal hypertrophic cardiomyopathy and nemaline myopathy associated with ACTA1 K336E mutation. Neuromuscul Disord. 2006; 16:548–552. [PubMed: 16945537]
34. Ishibashi-Ueda H, Imakita M, Yutani C, Takahashi S, Yazawa K, Kamiya T, Nonaka I. Congenital nemaline myopathy with dilated cardiomyopathy: an autopsy study. Hum Pathol. 1990; 21:77–82. [PubMed: 2295510]
35. Saffitz JE. Desmosome mutations in arrhythmogenic right ventricular cardiomyopathy: important insight but only part of the picture. Circ Cardiovasc Genet. 2009; 2:415–417. [PubMed: 20031615]

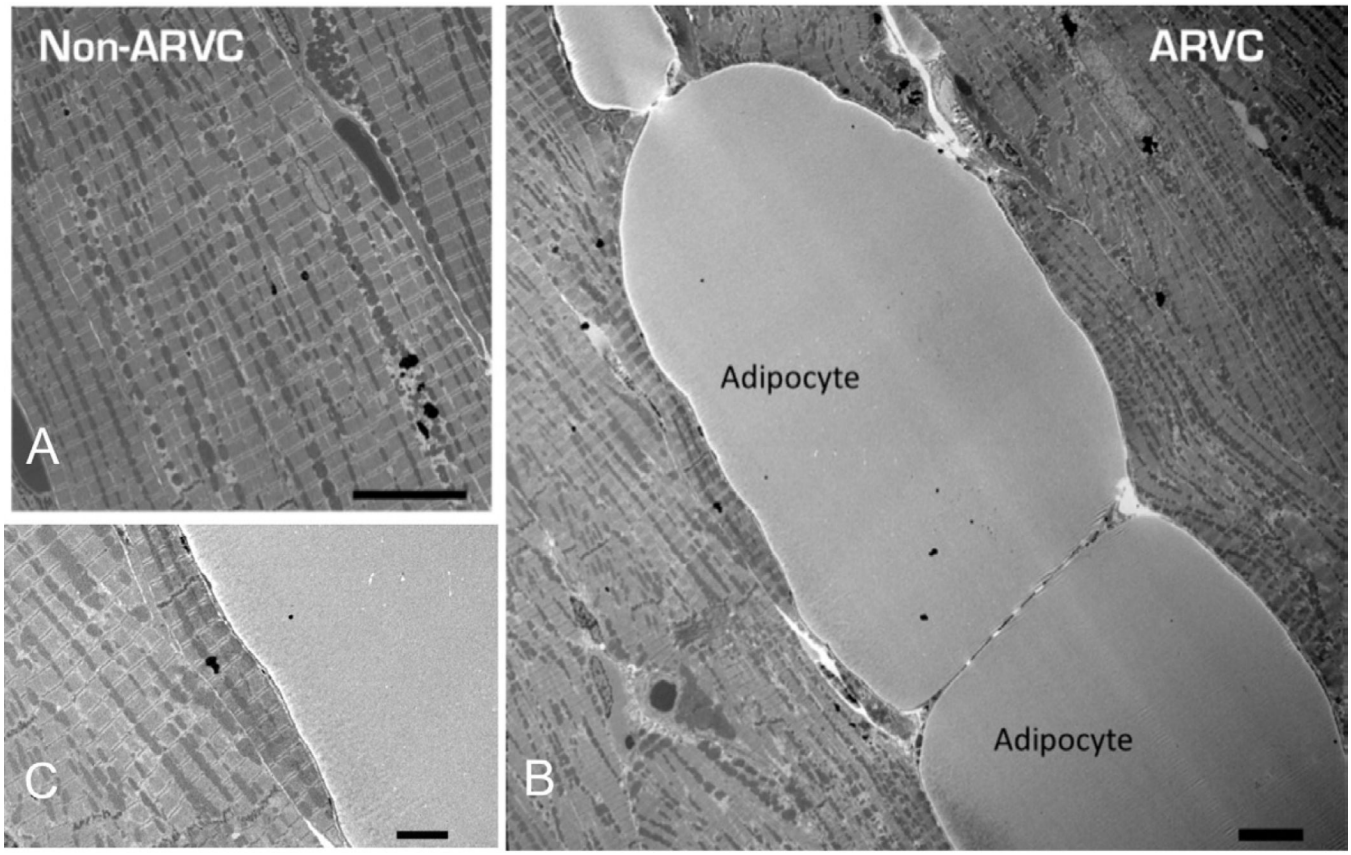

Figure 1.
1900X magnification electron micrographs of cardiac tissue from non-ARVC (Panel A) and ARVC (Panel B) canines. ARVC image reveals infiltration of adipocytes within the myocardium. No junctions were observed between myocytes and adipocytes (Panel C). Scale bars denote 10 μm in Panel A and B, and 1 μm in Panel C.

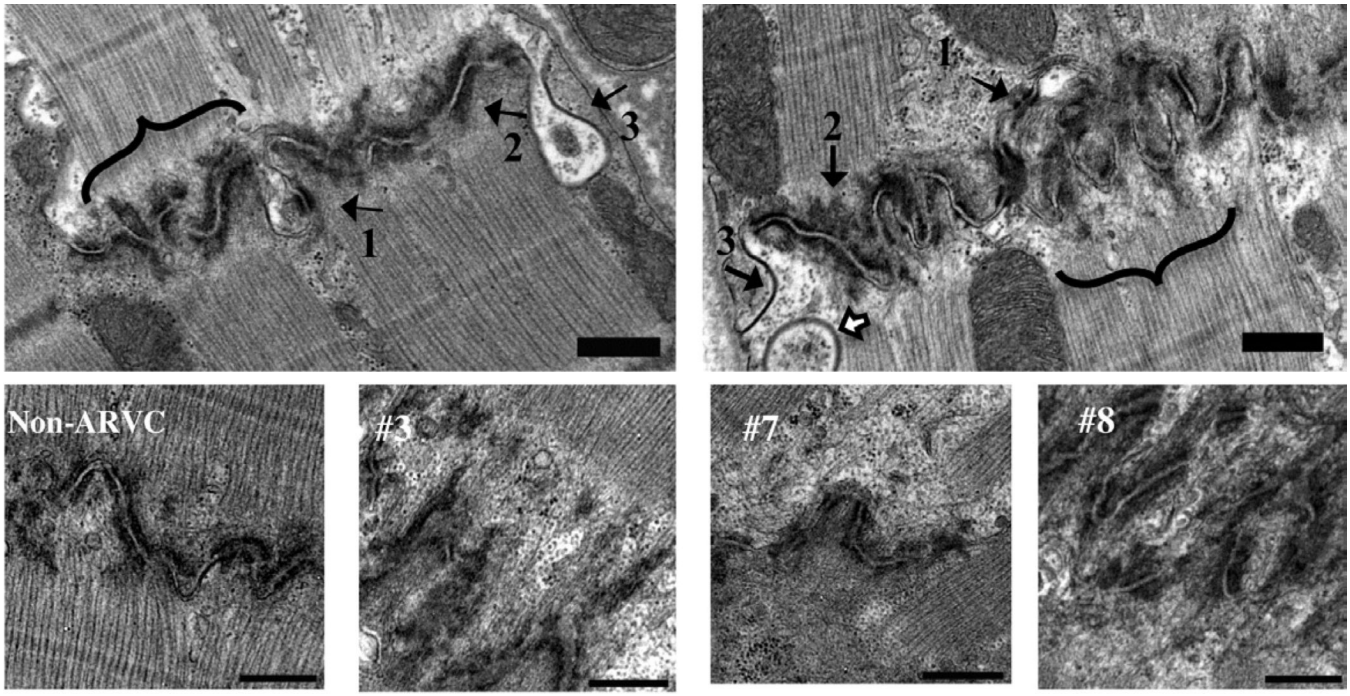

Figure 2.

13000X (scale bar denotes 500nm) electron micrographs of intercalated discs from non-ARVC (left panel) and ARVC (right panel) afflicted tissue. Arrow 1: desmosome, arrow 2: adherens junctions, arrow 3: gap junction. White arrow, top right panel: Annular gap junction. Adjacent to the intercalated disc, pale areas lacking filaments are apparent in ARVC afflicted samples (bracket). Comparable areas in controls appeared more electron dense and included filaments (bracket). Bottom panels show images of midmyocardial RV at 13000X magnification. One non-ARVC (left) and 3 ARVC dogs (#3, 7, 8) are included. Poorly organized, heterogeneous material, with actin filaments ending 0.25 to 1.5 microns away from the membrane of the cell were present rarely in non-ARVC, and commonly in ARVC afflicted dogs. Dog #8 (lower, far right panel) revealed disorganized and folded intercalated discs.

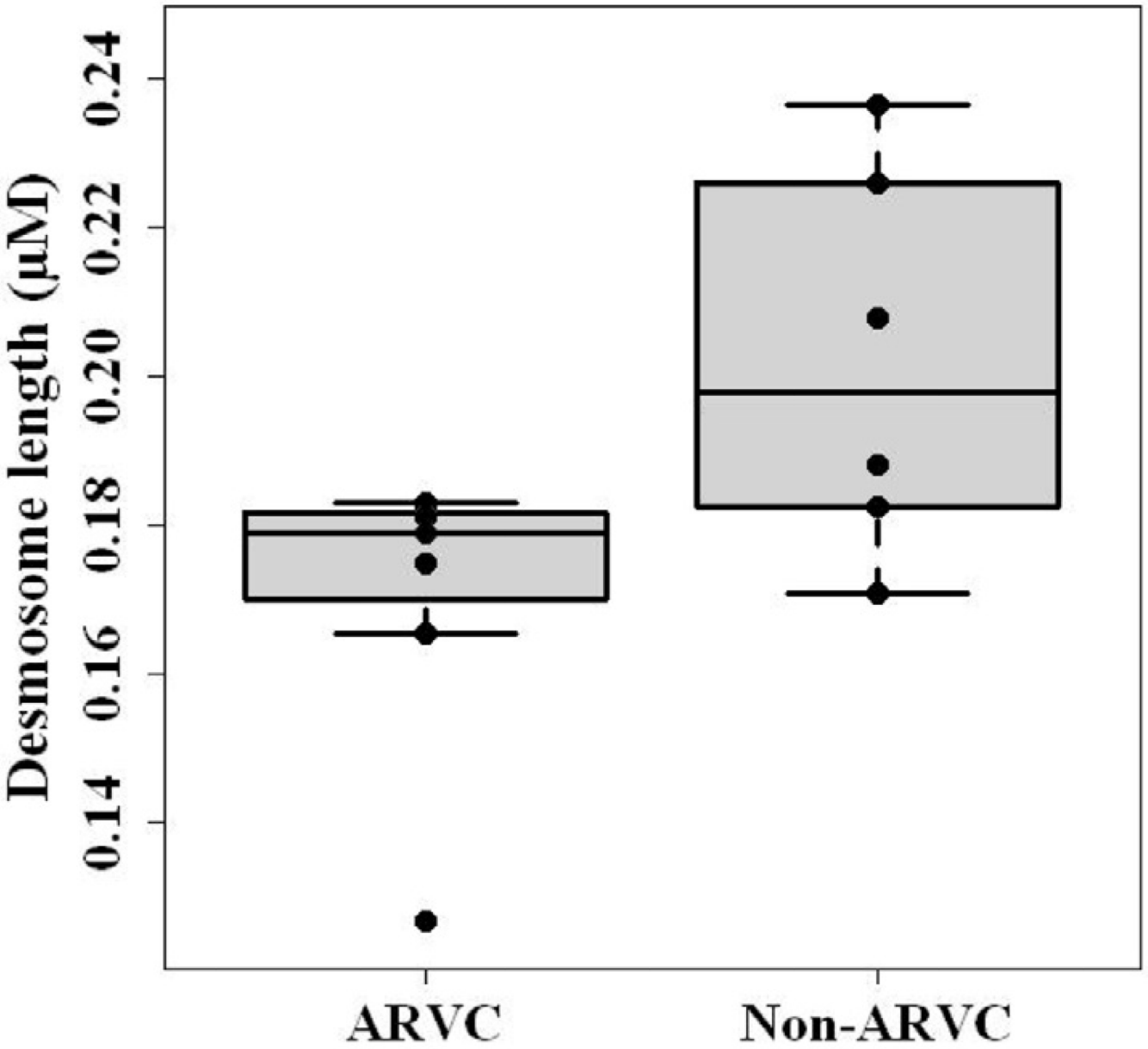

Figure 3.

Box-and-whiskers plot compares desmosome length in the LV of ARVC and non-ARVC dogs. The black line dividing the box denotes median (ARVC, 0.18; Non-ARVC, 0.20), the bottom and top of the box show the 25th and 75th percentile, and whiskers denote the maximum and minimum points that lie within 1.5 times the interquartile range. ARVC Range, 0.13–0.18; Non-ARVC Range, 0.17–0.24. All points are shown. A significant reduction in the length of desmosomal plaques was found in the LV of ARVC dogs (P=0.04).

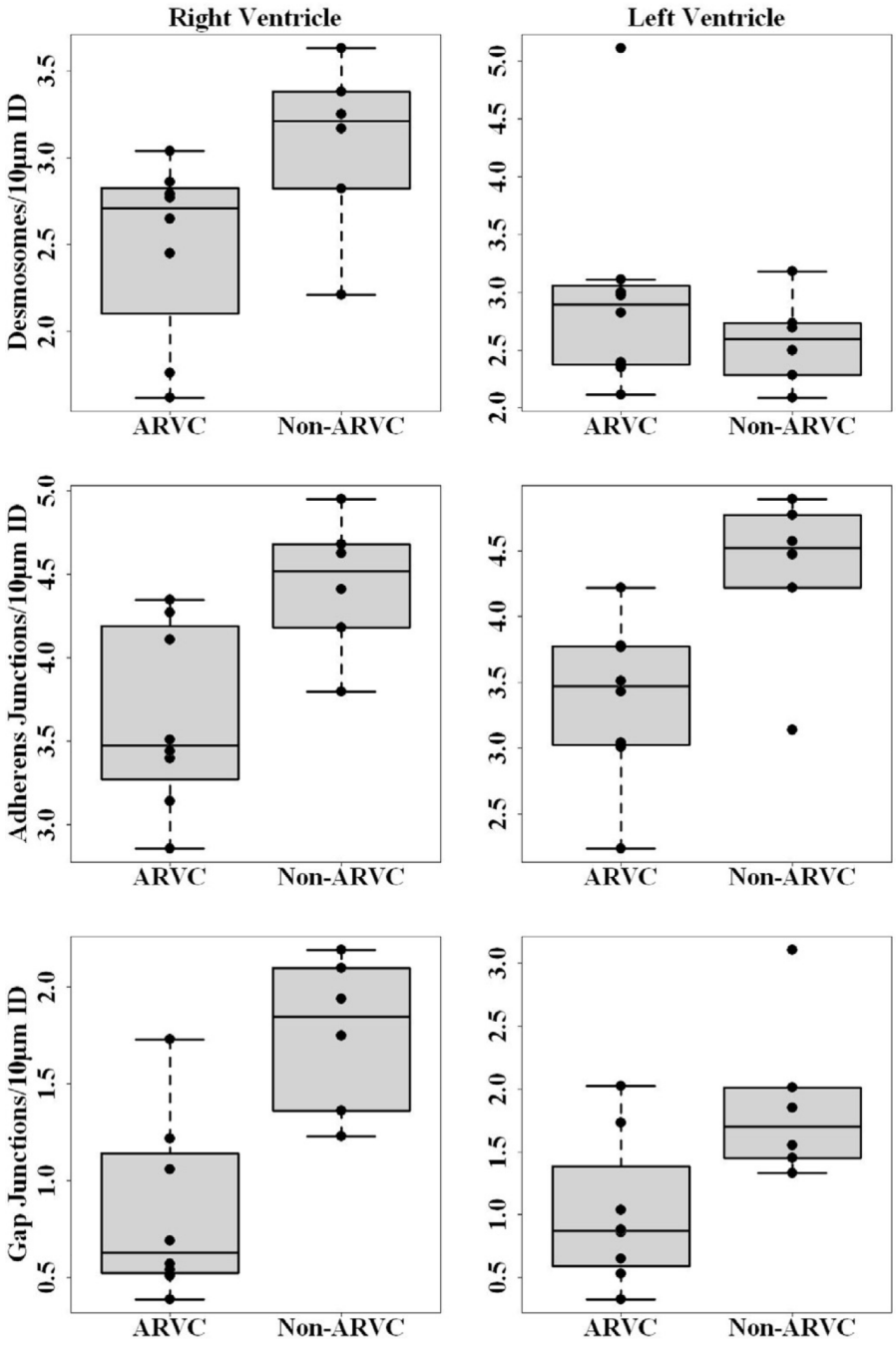

Figure 4.

Box-and-whiskers plots compare desmosomes (top panel), adherens junctions (middle panel), and gap junctions (bottom panel) per 10 microns of intercalated disc in RV (left column) and LV (right column) of ARVC and non-ARVC dogs. Black lines across each plot denote the median, the bottom and top of each box represents the 25th and 75th percentile, and whiskers show the maximum and minimum points within 1.5 times the interquartile range. All individual points are shown. Significant reduction in the number of desmosomes/10 microns of intercalated disc was found in RV (P=0.04, ARVC: Median, 2.71, range, 1.62–3.04; Non-ARVC: Median, 3.21, Range, 2.21–3.63), while no significant reduction was detected in LV (P=0.88, ARVC: Median, 2.90, Range, 2.11–5.11; Non-ARVC: Median,

2.60, Range, 2.09–3.18). Significant reduction of adherens junctions/10 microns of intercalated disc were detected in both RV and LV [RV: *P*=0.04 (ARVC: Median, 3.48, Range, 2.86–4.35; Non-ARVC: Median, 4.52, Range, 3.80–4.95, LV: *P*=0.04 (ARVC: Median, 3.47, Range, 2.24–4.22; Non-ARVC: Median, 4.52, Range, 3.14–4.89)]. Finally, a significant reduction in the number of gap junctions per 10 microns of intercalated disc was detected in both RV and LV of ARVC afflicted samples [RV: *P*=0.02, (ARVC: Median, 0.63, Range, 0.39–1.73; Non-ARVC: Median, 1.85, Range, 1.23–2.19) LV: *P*=0.04 (ARVC: Median, 0.87, Range, 0.33–2.02; Non-ARVC: Median, 1.70, Range, 1.33–3.10)].

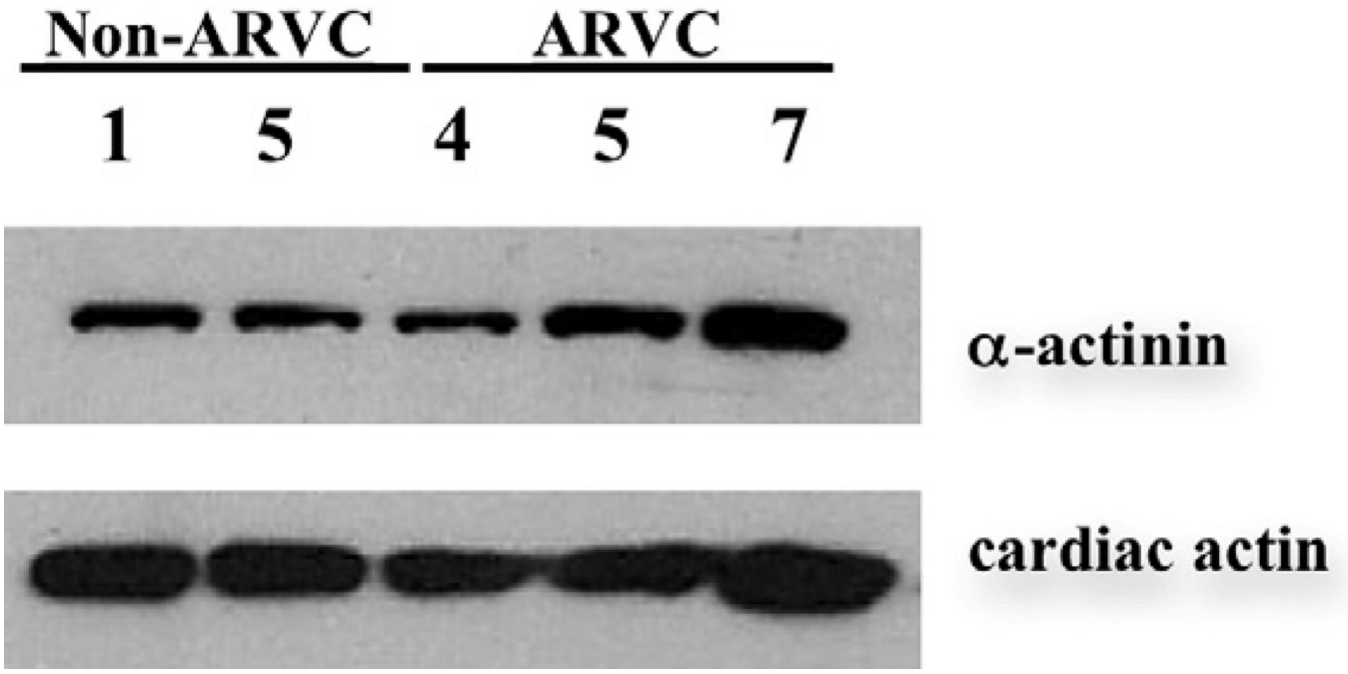

Figure 5.
Western blot for α-actinin. No difference in the amount of α-actinin was detected between 2 non-ARVC dogs (#1 and 5), and 3 ARVC boxers (# 4, 5, and 7). Cardiac actin served as a loading control.

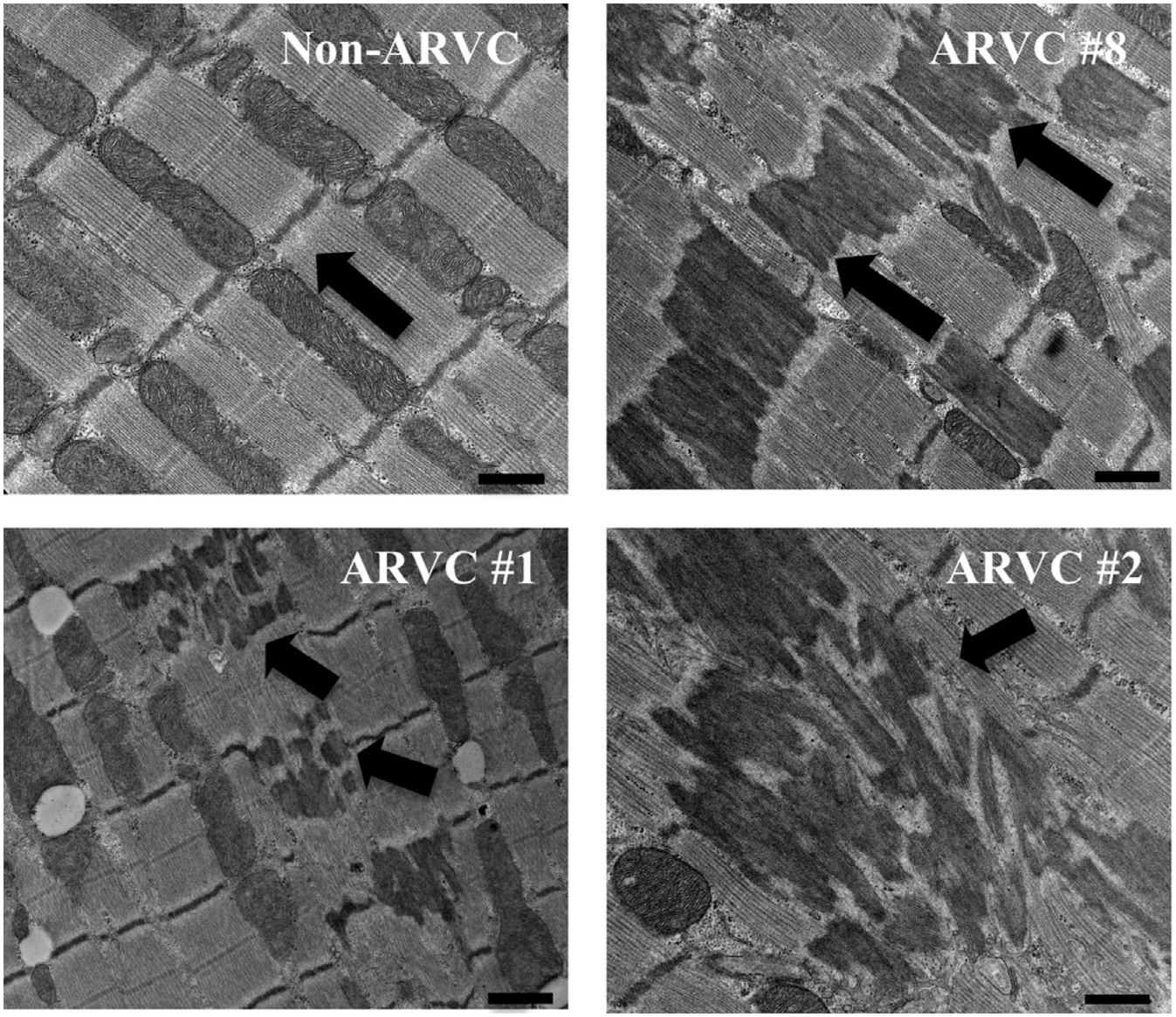

Figure 6.

Electron micrographs showing representative images of myocardium from a non-ARVC dog (dog 5), and 3 ARVC dogs (clockwise from top right: dog 8, 2, 1). In non-ARVC canines, proper alignment of the myofibrils, sarcomeres, and mitochondria were present. Z bands were aligned, denoting either end of the sarcomeres (black arrow). In ARVC afflicted samples, electron dense rods were present in 3 patterns (black arrows): First, comprising the length of every other sarcomere (#8). Second, in multidirectional clusters (#2). Third, originating from the Z band on either end of the sarcomere, and not present in the center (#1). Scale bars denote 500nm.

Table 1

Clinical summary of 24-hour Holter recordings and echocardiography in dogs with and without arrhythmogenic right ventricular cardiomyopathy (ARVC)

Signalment					24-hour Electrocardiography				Echocardiography					
Dog ID	**Breed**	**Sex**	**Wt (kg)**	**Age (yrs)**	**Ave HR (bpm)**	**Total VT**	**Total VE**	**%VE (%)**	**FS (%)**	**LA/Ao**	**LVDD (mm)**	**LVSD (mm)**	**LVFWd (mm)**	**IVSd (mm)**
ARVC														
1	Boxer	F	36.0	6.3	89	3	3,927	3	24.0	1.9	38.6	29.3	9.4	10.9
2	Boxer	Mc	22.8	5.2	NA	NA	NA	NA	31.2	1.8	39.6	27.3	8.6	10.7
3	Boxer	Mc	35.0	11.9	111	3745	26217	29	30.9	1.8	43.3	30.0	14.8	11.5
4	Boxer	M	33.5	9.2	93	47	67	<1	36.0	1.8	44.5	28.5	9.0	9.0
5	Boxer	Fs	26.0	5.5	100	1,252	22,788	16	9.9	1.5	39.4	35.5	10.5	12.9
6	Boxer	Mc	31.1	10.0	79	0	234	<1	28.0	1.7	37.4	26.9	13.3	11.3
7	Boxer	M	36.1	12.0	113	17,688	56,990	35	26.2	2.1	45.5	33.6	11.6	11.0
8	Boxer	Mc	34.5	9.0	90	42,143	43,120	30	20.4	1.8	39.6	31.5	8.9	11.5
Non-ARVC														
1	Beagle	F	NA	5.0	NA	NA	NA	NA	NA	NA	NA	NA	NA	NA
2	GS	F	31.3	13.0	85	0	4	<1	36.6	1.3	23.9	8.9	9.4	9.5
3	GS	F	21.5	7.5	90	0	15	<1	35.7	1.3	37.3	24.0	11.2	9.3
4	GS	F	NA	4.0	87	0	2	<1	36.8	1.7	46.5	29.4	11.1	10.8
5	GS	F	18.5	5.5	78	0	4	<1	33.7	1.5	37.1	24.6	10.1	10.4
6	GS	M	27.3	5.5	78	0	63	<1	37.1	1.3	38.3	24.1	14.0	9.6

ID, identity; Wt, weight; Ave HR, average heart rate; bpm, beats per minute; VT, ventricular tachycardia; VE, ventricular ectopy; FS%, fractional shortening percent; LA/Ao, left atrial to aortic ratio; LVDD, left ventricular end-diastolic dimension; LVSD, left ventricular end-systolic

Table 2

Outline of procedures that were performed on particular dogs in this study.

Dog ID	Breed	Holter	Echocardiography	Gross pathology and Histopathology	Electron microscopy	Western blot	Trapezius examination
ARVC 1	Boxer	X	X	X	X	NA	X
ARVC 2	Boxer	NA	X	X	X	NA	NA
ARVC 3	Boxer	X	X	X	X	NA	NA
ARVC 4	Boxer	X	X	X	X	X	NA
ARVC 5	Boxer	X	X	X	X	X	X
ARVC 6	Boxer	X	X	X	X	NA	X
ARVC 7	Boxer	X	X	X	X	X	NA
ARVC 8	Boxer	X	X	X	X	NA	NA
Non ARVC 1	Beagle	NA	NA	NA	X	X	X
Non ARVC 2	GSD	X	X	X	X	NA	NA
Non ARVC 3	GSD	X	X	X	X	NA	X
Non ARVC 4	GSD	X	X	X	X	NA	NA
Non ARVC 5	GSD	X	X	X	X	X	NA
Non ARVC 6	GSD	X	X	X	X	NA	NA

"X" denotes that procedure was completed. "NA" indicates the study was not available for that dog.